Particle & Particle Systems Characterization
www.particle-journal.com

Review of Sn-Doped Hematite Nanostructures for Photoelectrochemical Water Splitting

*Yichuan Ling and Yat Li**

Hematite (α-Fe_2O_3) nanostructures have been extensively studied as photoanodes for photoelectrochemical (PEC) water splitting. However, the photoactivity of pristine hematite nanostructures is limited by a number of factors, including poor electrical conductiviy and slow oxygen evolution reaction kinetics. Previous studies have shown that using tin (Sn) as an n-type dopant can substantially enhance the photoactivity of hematite photoanodes by modifying their optical and electrical properties. Here, the recent accomplishments in using Sn-doped hematite photoanodes for solar water splitting are highlighted.

1. Introduction

Solar water splitting is an environmentally friendly reaction of producing hydrogen gas.[1–9] Since Honda and Fujishima first demonstrated solar water splitting in 1972 by using semiconductor titanium dioxide (TiO_2) as photoanode in a photoelectrochemical (PEC) cell,[7] extensive efforts have been invested into improving the solar-to-hydrogen (STH) conversion efficiency and lower the production cost of photoelectrochemical devices. The "Z-scheme" photoelectrochemical device consists of a photoanode and a photocathode has been demonstrated to be a promising approach to achieve direct water splitting (**Figure 1**).[9–13] In a Z-scheme device, the photocurrents of photocathode and photoanode have to be matched in order to get the optimal performance. In the last few years, researchers have made significant progress in developing high performance photocathodes. For example, it has been reported that Rh-modified single-crystal InP achieved a STH efficiency of 13%.[14,15] Besides, planar Pt/n^+p-Si photocathodes achieved a remarkable photocurrent of ≈30 mA cm^{-2} under one sun illumination, which is close to 10% STH conversion efficiency.[16] On the other hand, photoanodes still have relatively lower photocurrent density, which limits the overall efficiency for direct water splitting.[9–11]

A number of n-type semiconductors, such as TiO_2,[7,17–26] ZnO,[27–34] WO_3,[35–41] and $BiVO_4$,[13,37,42–53] have been studied as photoanode materials for water splitting. Among them, hematite is one of the most attractive materials for photoanode.[1,2,54–58] Hematite has a favorable optical bandgap around 1.9–2.2 eV[59] for harvesting solar light, which corresponding to a high theoretical STH conversion efficiency of 14%–17%.[60] Iron is the fourth most abundant element in the Earth's crust (6.3% by weight),[5] and hematite is a low-cost material. In addition, hematite is chemically stable in solutions of different pH.[61] However, the STH conversion efficiencies of reported hematite photoanodes are considerably lower than the theoretical value, owing to its very short-excited state lifetime (<10 ps),[62] short hole diffusion length (≈2–4 nm),[5,61] poor surface oxygen evolution reaction kinetics,[63] and poor electrical conductivity (10^{-6} Ω^{-1} cm^{-1}).[5]

The recent development of hematite nanostructures, including nanoparticles,[59,64,65] nanowires[66,67] and nanonets,[56,58] opens up new opportunities in addressing the abovementioned limitations. Nanostructured photoanode offers increased semiconductor/electrolyte interfacial area for water oxidation, as well as substantially reduced diffusion length for minority carriers. Therefore, nanostructured hematite photoelectrodes are expected to be more efficient in charge carrier collection than their bulk counterparts.[60] For example, Lin et al. reported the growth of ultrathin hematite film (25 nm) on a conductive nanonet structure. The nanonet-based hematite photoanode achieved an excellent photocurrent of 1.6 mA cm^{-2} at 1.23 V versus RHE, which is four times higher than the value obtained from the planar sample with the same thickness. The photocurrent enhancement was due to the increased activation sites for water oxidation (**Figure 2**).[56]

To further improve the photoactivity of hematite photoanode, element doping has been extensively studied to improve the structural, electronic and optical properties of hematite. The role of dopants, such as Ti,[65,68–75] Si,[68,76–79] Al,[71,80] Mg,[81,82] Zn,[71,78] Be,[80] Mo,[83] and Sn,[4,61,69,80,81,84–90] on the PEC performance of hematite have been investigated. Recently, there is an increasing interest of developing Sn-doped hematite nanostructured photoanode due to the significant effect of Sn doping on the photoactivity of hematite. Sn^{4+} is a tetravalent dopant that can be substitutionally doped into hematite at the Fe^{3+} sites.[69,71,89] The electrical conductivity of Sn-doped hematite is enhanced by the occurrence of bivalent ions, Fe^{2+}. The local pairs of Fe^{2+}–Sn^{4+} play a role as donor centers in the hematite, causing enhanced electroconductivity.[84] In this article, we will review the recent progress in the synthesis of Sn-doped nanostructured hematite materials and their implementations as photoanodes for water splitting. The influence of Sn doping on the photoactivity of hematite photoanodes will also be discussed.

Y. Ling, Prof. Y. Li
Department of Chemistry and Biochemistry
University of California
Santa Cruz, CA 95064, USA
E-mail: yatli@ucsc.edu

DOI: 10.1002/ppsc.201400051

2. The Effect of Sn Doping on the Optical and Electronic Properties of Hematite

It has been reported that Sn doping can significantly affect the optical and electronic properties of hematite. Due to the size difference between Sn^{4+} (0.69 Å) and Fe^{3+} (0.65 Å) cations, the substitutional incorporation of Sn^{4+} ions can induce a slight structural distortion of hematite unit cell, and thus affects the optical properties of hematite.[4] Sivula et al. reported that this structural distortion of the hematite lattice combined with the increased particle size can increase the absorption coefficient of hematite by a factor of 2.[4] Moreover, the n-type Sn^{4+} substitution will also change the electronic properties of hematite, which plays an important role in determining the photoactivity of hematite. As an electron donor, the incorporation of Sn^{4+} is expected to substantially increase the electron density of hematite. The increase of carrier density can up shift the Fermi level of hematite and increase the band bending at the semiconductor/electrolyte interface, which could improves charge separation. Additionally, a more electrically conductive semiconductor electrode can reduce the energy loss due to the internal resistance of electrode and the contact resistance at the semiconductor/back contact interface.[9] The electronic structure calculation based on the first-principles calculations within the GGA+U approximation showed that Sn-doped hematite exhibits an improved electrical conductivity due to the reduction of electron effective mass at the conduction band minimum.[91] Heavily Sn-doped hematite also appears to have a reduced bandgap, which leads to enhanced utilization ratio of solar energy and the expansion of optical absorption scope.[91]

The first attempt to study the PEC performance of Sn-doped hematite was reported by Kennedy et al.[61] in 1981. They reported that hematite photoelectrodes doped with group IVA elements, Si, Sn, and Ge, showed better photocurrents over that Ti doped hematite. In 2007, Aroutiounian et al.[84] carried out the investigation of the PEC properties of the ceramic polycrystalline Sn-doped (up to 2% Sn ratio) hematite photoelectrodes. The Sn-doped hematite photoelectrodes were made via solid-phase reaction by sintering the mixture of Fe_2O_3 and SnO_2 in the air at ≈1100 °C for 7 h, followed by pressing the mixed powders into compact pellets and sintering again at ≈1300 °C for 25 h. The results showed that photoelectrodes with 0.75%–1% Sn-doping have a high donor density, reasonably flat band energy levels, and the highest incident photon-to-current efficiency values. In 2009, Jang et al.[80] reported the study photoelectrochemical properties of Sn-doped hematite using scanning electrochemical microscopy (SECM). By using this screening method, arrays of doped materials can be rapidly screened to determine if the photocatalysts are sensitive to UV or visible light irradiation. Hematite co-doped with Sn and Be (or Al) showed an improved photocurrent response. Jang et al.[86] also investigated the effect of Sn doping in Sn-doped Ag-Fe_2O_3 nanocomposite photocatalyst using the same SECM method. Amongst the samples with different doping concentrations, 2% Sn-doped Ag-Fe_2O_3 nanocomposite exhibited the highest photocurrent in alkaline solution under visible light irradiation ($\lambda \geq 420$ nm). These results revealed the potentials of Sn-doped hematite materials as photoanodes for PEC water splitting. However, the reported photocurrent densities in these pioneer works were only on the order of μA cm^{-2}. The poor photoactivity of these Sn-doped hematite photoelectrodes was attributed to the significant electron-hole recombination loss in the thick hematite film. In 2010, Sivula et al. incorporated Sn-doping into nanostructure hematite, which achieved a breakthrough in improving the PEC performance of Sn-doped hematite. A large increase of photocurrent (from ca. 10 μA cm^{-2} to 0.56 mA cm^{-2} at 1.23 V vs reversible hydrogen electrode, RHE) was achieved by thermally annealing the nanocrystalline hematite electrode at a sufficiently high temperature (800 °C).[4] Thereafter, numerous studies of Sn-doped hematite photoanodes have been reported. In the following sections of this article, we will focus primarily on recent progress in the synthesis and characterization of element-doped nanostructured hematites and their performance as PEC photoanodes for water splitting.

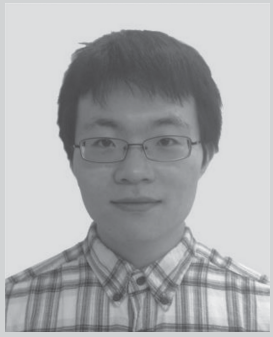

Yichuan Ling is currently a fifth year chemistry Ph.D. student at University of California, Santa Cruz, under the supervision of Prof. Yat Li. He received his B.S. in chemistry from Fudan University, China in 2009. His research focuses on the synthesis of hematites and III-V semiconductor nanomaterials and the investigation of their applications in solar energy conversion.

Yat Li received his B.S. and Ph.D. in chemistry from the University of Hong Kong. He was a postdoctoral research fellow at Harvard University from 2003 to 2007 under the supervision of Prof. Charles M. Lieber. He moved to the University of California Santa Cruz in 2007 and is now an associate professor of chemistry. His research focuses on the design and synthesis of semiconductor nanostructures, the investigation of their fundamental properties, and the exploration of their potential for solar energy conversion and storage.

3. Unintentional Sn Doping via High Temperature Annealing

In 2010, Sivula et al.[4] reported the growth of nanocrystalline hematite on fluorine-doped tin oxide (FTO) substrates using a solution-based colloidal method. The 5 to 10-nm-size hematite nanoparticles were synthesized by thermal decomposition of $Fe(CO)_5$. The hematite electrodes annealed at 700 °C or below exhibited minimal photoactivity for water splitting (**Figure 3**a). In contrast, hematite photoanode annealed at 800 °C achieved

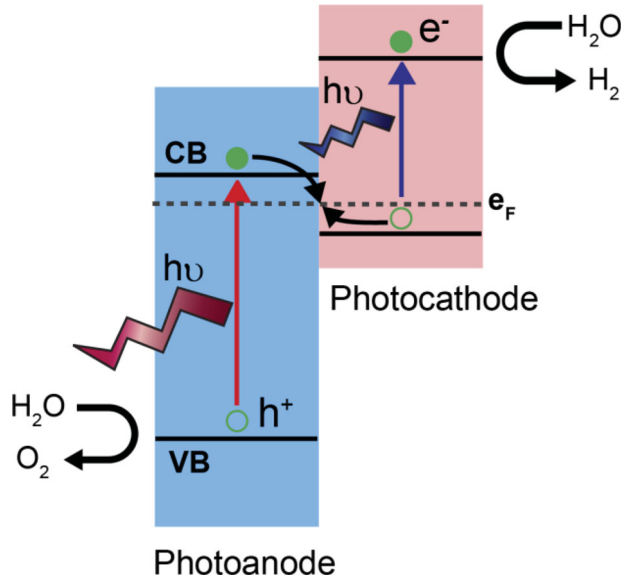

Figure 1. Schematic illustration of a Z-scheme photoelectrochemical device. Solid and empty circles represent photoexcited electrons and holes.

an excellent photocurrent of 0.56 mA cm^{-2} at 1.23 V vs RHE under one sun illumination. X-ray photoelectron spectroscopy (XPS) analysis suggested that the Sn^{4+} were incorporated into hematite nanostructures upon high temperature annealing (800 °C). The substitutional Sn^{4+} doping increased the optical absorption coefficient of the hematite nanostructure as a result of lattice distortion (Figure 3b), and thus, increased the photoactivity of hematite photoanode.[4]

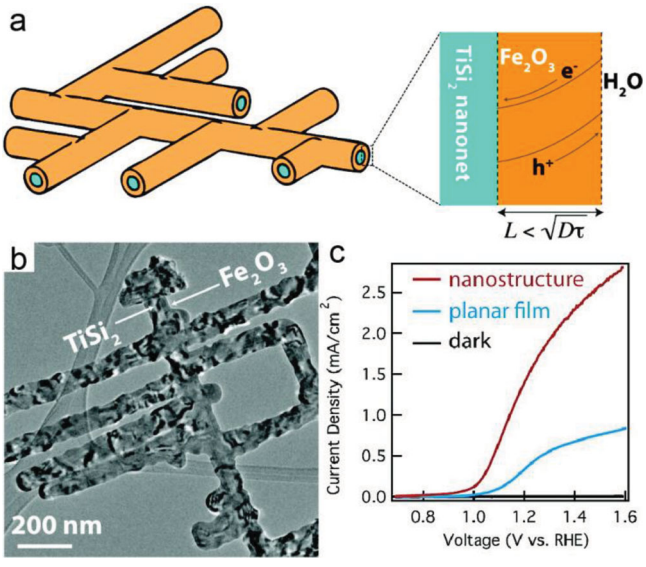

Figure 2. a) Schematic illustration of the design nanonet-based hematite, which involves the use of a highly conductive $TiSi_2$ nanonet as an effective charge collector. The electronic band structure is shown in the enlarged cross-sectional view. Efficient charge collection is achieved when the hematite thickness is smaller than the charge-diffusion distance. b) Transmission electron microscopy (TEM) image of a $TiSi_2$ core/hematite shell nanonet structure. c) Current density–voltage (*I*–*V*) curves of a $TiSi_2$ core/hematite shell structure and a planar hematite film. Reproduced with permission.[56] Copyright 2011, American Chemical Society.

Ling et al.[87] used this high-temperature annealing method on single crystalline hematite nanowires to study the influence of Sn doping on the electronic properties of hematite. Akaganeite (β-FeOOH) nanowires were first prepared on the FTO substrate by thermal hydrolysis of $FeCl_3$ (0.15 M) in a pH 1 solution containing 1 M $NaNO_3$ at 95 °C for 4 h. The as-prepared β-FeOOH-coated substrates were sequentially sintered in air at 550 °C for 2 h to obtain hematite nanowires. To achieve Sn doping, the hematite nanowires were further annealed at high temperatures ranging from 600 to 850 °C in air for an additional 20 min.[87] XPS data revealed that the diffusion of Sn from FTO substrate into the hematite nanostructure occurs when the annealing temperature is 650 °C or above (**Figure 4**a). The Sn/(Sn+Fe) atomic ratios (Sn%) of these unintentionally Sn-doped hematite nanowire samples increased with sintering temperature (**Table 1**). At the same time, the photocurrent densities of these hematite nanowires drastically increased with the sintering temperature (Figure 4b). The results proved that there is a strong correlation between the photoactivity of hematite and the Sn concentration. The hematite photoanode sintered at 800 °C exhibited an excellent photocurrent density of 1.24 mA cm^{-2} at 1.23 V vs RHE. Figure 4c shows the incident-photon-to-current-efficiencies (IPCE) of unintentionally Sn-doped hematite nanowires sintered at 650 and 800 °C collected at 1.23 V vs RHE. The 800 °C annealed hematite nanowires exhibited significantly enhanced IPCE values compared to the sample annealed at 650 °C in the entire 350 to 600 nm wavelength region. The enhanced photocurrent density was attributed to the increased electrical conductivity as a result of the incorporation of substitutional Sn-dopant diffused from the FTO substrate. The Mott–Schottky studies proved that hematite sample sintered at 800 °C has substantially increased donor density (5.38×10^{19} cm^{-3}) compared with the sample sintered at 650 °C (1.89×10^{19} cm^{-3}) (Figure 4d).

Recently, Morrish et al.[88] demonstrated a method to reduce the annealing temperature for the activation of Sn-doped hematite photoanode (**Figure 5**a). They found that the activation of PEC performance of hematite nanorod arrays can be achieved using a rapid annealing process (5 min) at high temperature (750 °C), or after a long-time (8 h) annealing process at a lower temperature (600 °C) (Figure 5b). A lower annealing temperature is of practical significance because it can reduce the damage to the structure and electrically conductivity of FTO substrate and reduce the energy cost of the annealing process.

A detailed study of Sn diffusion from FTO substrate into hematite was carried out by Bohn et al.[92] Sputter-deposited hematite films (of thickness 600 nm) on FTO-coated glass and annealed at 500 °C (2 h) and 800 °C (10 min) were investigated (**Figure 6**a). Direct evidence of the Sn dopant being incorporated into hematite from the FTO was quantitatively observed using secondary ion mass spectrometry (SIMS) (Figure 6b). By investigating the composition of the cross sections of sputtered hematite film, the average molar fraction of Sn over the first 100 nm of material in the sampled at 800 °C was found to be approximately 0.02%, which was an order of magnitude higher than that of the sample annealed at 500 °C. The SIMS studies confirmed that Sn can diffuse from the FTO substrate to the

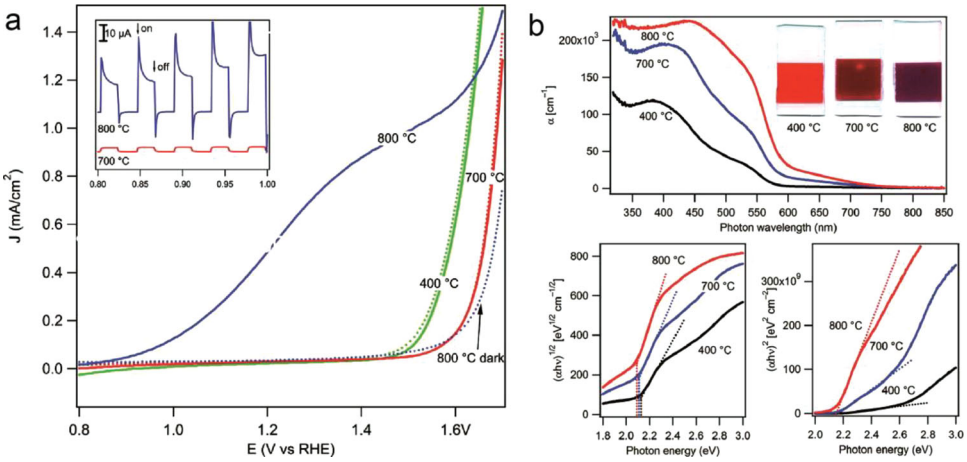

Figure 3. a) Electrochemical water oxidation current vs voltage curves of the photoanodes sintered at different temperatures in the dark (dotted curves) and under simulated solar light (solid curves). The inset shows the photocurrent transient curves for the 700 and 800 °C sample created by chopping the light source during a current vs voltage sweep. b) Optical properties of mesoporous hematite thin films. Top graph: shows the absorption coefficient as a function of wavelength and the typical appearance of the electrodes. Tauc plots evaluating the optical bandgap are shown for the indirect case (lower left graph) and the direct case (lower right graph). A dotted line fitted to the linear portion of these plots shows the optical bandgap approximation. Reproduced with permission.[4] Copyright 2010, American Chemical Society.

hematite. The influence of Sn-doping on hematite's electronic properties was studied by the Mott–Schottky technique and conductivity measurement. The results showed the donor density of Sn-doped hematite annealed at 800 °C is two orders of magnitude higher than undoped sample. The enhanced donor density results in a five times reduced resistance for the Sn-doped hematite sample.

4. Intentionally Sn-Doped Hematite Nanostructures

Although high-temperature sintering has been proven to be an effective method to introduce Sn dopant into hematite nanostructures, it is certainly not ideal because the high-temperature process will considerably degrade the electrical conductivity of the FTO substrate. Ling et al.[87] reported the growth of intentionally Sn-doped hematite nanostructures on a conducting substrate via a hydrothermal method using $SnCl_4$ ethanol solution as the Sn precursor. The Sn-doped hematite had coral-like nanostructures constituted by small nanorods, with an average diameter of ≈40 nm and a length of ≈100 nm revealed by SEM images (**Figure 7**a). XPS analysis confirmed that the intentionally Sn-doped hematite nanocoral structure has higher Sn concentration than the unintentional Sn-doped hematite that annealed at the same temperature. The Sn-doped nanocoral samples also showed a higher photocurrent density than the unintentionally Sn-doped nanowire sample (Figure 7b). This work demonstrated a simple and effective preparation procedure for intentionally Sn-doped hematite.

Subsequent effort has been devoted to studying the amount of Sn doping in nanostructured systems that is required to achieve optimal PEC performance. Uchiyama et al.[89] tested a series Sn-doped hematite photoanodes with different Sn/(Fe+Sn) mole ratios from 0% to 100% (denoted as Sn0 to Sn1.0). Sn-doped hematite films were prepared by repeating the dip-coating-and-heating process, followed by annealing at 700 °C for 10 min in air. The products were a mixture of Sn-doped hematite and SnO_2. The SEM studies showed that the morphologies of hematite films became smoother with the increase of Sn-doping (**Figure 8**a). The results indicated that the mole ratio of Sn is highly related to the surface area of hematite film. UV–visible light absorption spectra showed that the absorbance decreased with increasing the amount of Sn (Figure 8b). The hematite samples with Sn amount less than 25% (Sn0, Sn0.1, and Sn0.25) showed diffraction peaks attributed to hematite in XRD patterns (Figure 8c), and the peaks shifted slightly to lower angles with increasing Sn atomic ratio. This was attributed to the lattice expansion due to the substitution of Fe^{3+} by Sn^{4+}, which has a larger ionic radius. Among all the samples, the highest photocurrent was achieved by the 10% Sn-doped hematite (Figure 8d). It was a balanced between the enhanced donor density, light absorbance, and surface roughness.

Another solution-based colloidal approach using mixed precursors has been reported by Frydrych et al.[90] A specific amount of anhydrous tin (II) chloride was added into the spin-coated ferric chloride solution in order to achieve controlled Sn doping. Varied Sn:Fe doping fractions from 0:100 to 20:100 were prepared by the spin-coating procedure. A relatively lower annealing temperature of 650 °C was used in this work to minimize the damage to the FTO glass substrate. SEM images demonstrated that with the increasing amount of Sn doping, the space between hematite particles became smaller. The photocurrent densities increased with the Sn doping fraction. The optimized sample with doping ration 20:100 achieved 0.45 mA cm^{-2} at 1.43 V vs RHE, suggesting that this spin-coating method was a simple and cost-effective preparation of active hematite photoanodes for PEC water splitting. This work showed that an optimum photoactivity for Sn-doped hematite nanostructure electrode can be achieved by manipulating the amount of Sn doping.

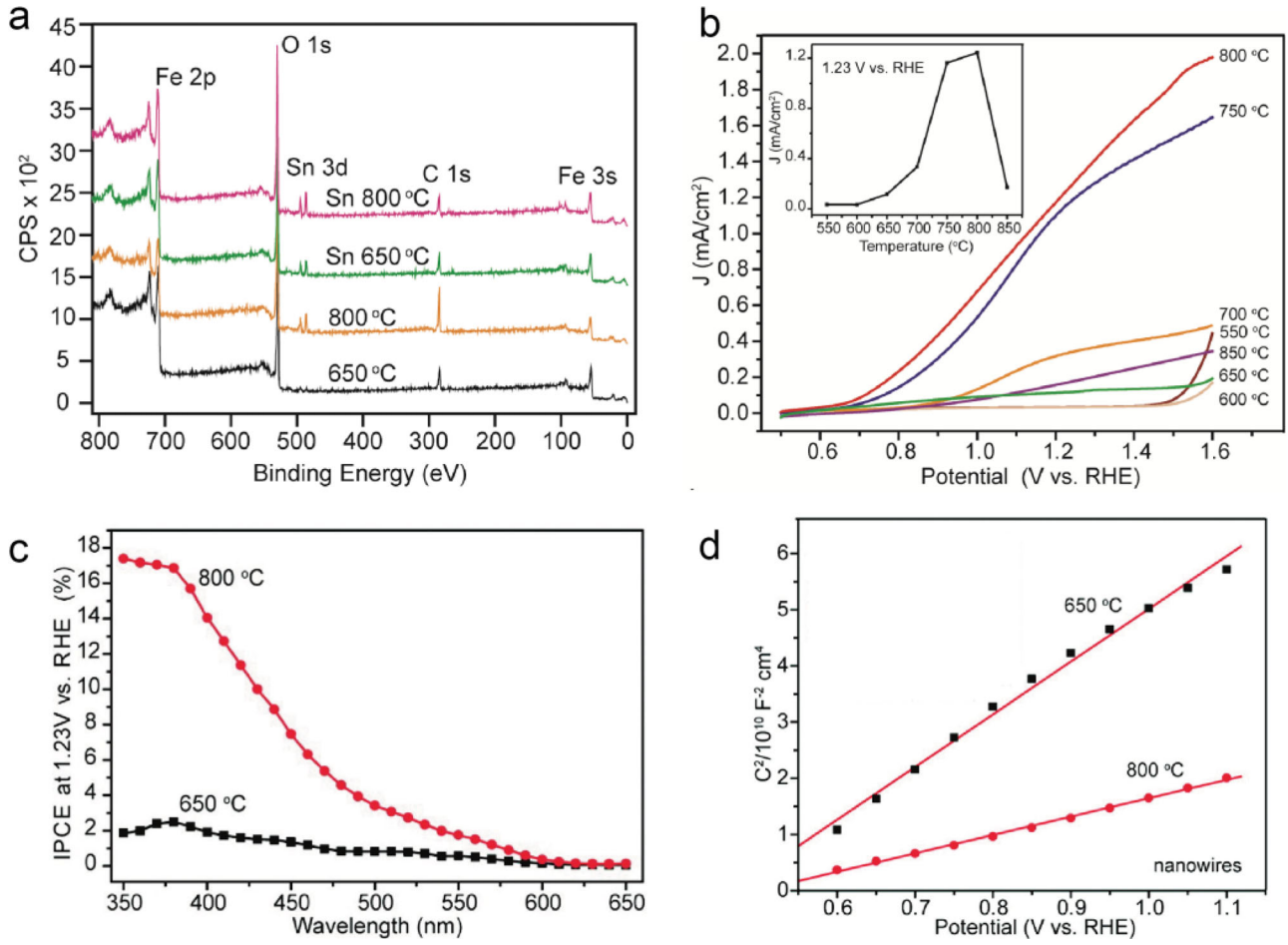

Figure 4. a) XPS survey of hematite nanowires and nanocorals sintered at 650 and 800 °C. b) *J–V* scans collected for hematite nanowire photoanodes sintered at different temperatures, with a scan rate of 10 mV s^{-1}. All samples were measured in 1 M NaOH electrolyte (pH 13.6) with the AM 1.5G simulated solar light at 100 mW cm^{-2}. Inset: photocurrent densities at 1.23 V vs RHE are plotted as a function of sintering temperature. c) IPCE spectra of hematite nanowire samples sintered at 650 and 800 °C, collected at the incident wavelength range from 350 to 650 nm at a potential of 1.23 V vs RHE. d) Mott–Schottky plots of hematite nanowires collected with a scan rate of 10 mV s^{-1}, in 1 M NaOH electrolyte (pH 13.6), in the dark at a frequency of 10 kHz. Reproduced with permission.[87] Copyright 2011, American Chemical Society.

5. Sn-Doping Through Post-Growth Surface Treatment

In the above-mentioned doping methods, the dopants are incorporated into hematite crystal during the process of material growth, which typically affects the material growth processes leading to changes of hematite morphologies, feature sizes, and thickness[87,89,90] For example, the addition of $SnCl_4$ into the hydrothermal process changed the hematite nanostructure from nanowires to nanocorals.[87] The recently demonstrated post-growth Sn doping methods can address this issue.[85] It is a facile doping strategy that is independent on the synthetic method of hematite and could potentially to be applied to any hematite nanostructures. Xi et al. reported dropping $SnCl_4 \cdot 5H_2O$ aqueous solution (5, 20, 60 × 10^{-3} M) as a Sn precursor directly on the hydrothermally grown FeOOH nanorod arrays film before subsequent annealing in air at 750 °C for 30 min. This chemical treatment introduces the Sn dopant into hematite and forms a 1–2-nm-thick layer of amorphous $Fe_xSn_{1-x}O_4$ at the interface of SnO_2 and hematite. Significantly, the photocurrent densities of these chemically treated hematite nanorod arrays increased from 1.24 for the pristine nanorods to 1.80 and 2.25 mA cm^{-2} at 1.23 V vs RHE with 5 and 20 × 10^{-3} M $SnCl_4$ treatments, respectively. Further increasing $SnCl_4$

Table 1. Summary of Sn 3d XPS data for hematite samples annealed at different temperatures.[87]

Temperature [°C]	550	600	650	700	800	850
Sn atomic ratio [%]	0	0	1.1	0.9	9.9	11.1

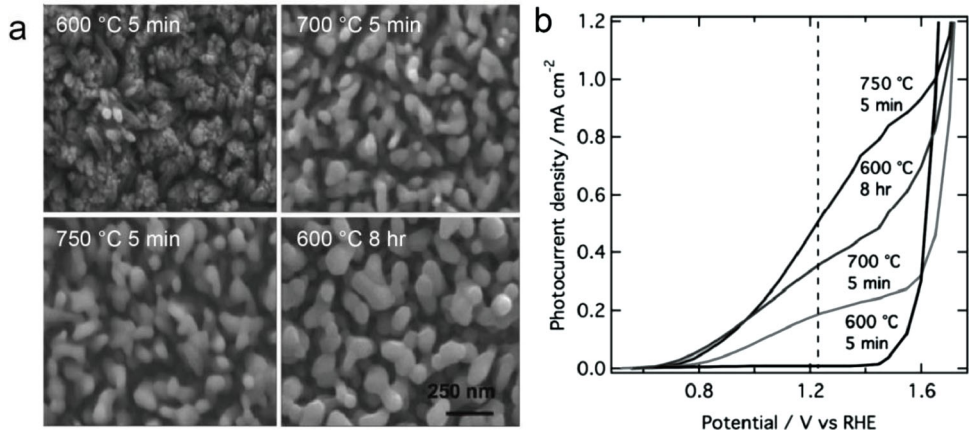

Figure 5. a) SEM images of hematite nanostructures for selected annealing conditions. The scale bar applies to all four images. b) Photocurrent density as a function of applied potential for hematite photoanodes annealed with the conditions described in (a). Reproduced with permission.[88] Copyright 2011, WILEY-VCH Verlag GmbH & Co. KGaA.

concentration to 60×10^{-3} M resulted in a thick $Fe_xSn_{1-x}O_4$ interfacial layer blocked the hole transport and leaded to a weaken photoactivity. The optimum concentration of Sn precursor solution was determined to be 20×10^{-3} M, as a thin $Fe_xSn_{1-x}O_4$ interfacial layer can reduce electron-hole recombination at hematite nanorods-electrolyte interface and increase the charge injection efficiency from the nanorods to electrolyte for water oxidation.[85] This work proved that $SnCl_4$ surface treatment is a facile strategy for doping Sn into hematite nanorods for enhanced photoactivity. The thin $Fe_xSn_{1-x}O_4$ layer facilitates the charge transfer through the hematite and suppresses electron-hole recombination at the semiconductor/electrolyte interface. This novel surface treatment shows great potential to be applied on hematite nanostructures with different morphologies.

6. Conclusions and Outlook

We have highlighted the recent progress in employing various methods for controlled incorporation of Sn into hematite, including unintentional Sn doping via high temperature annealing process, intentionally Sn doping by mixing Fe and Sn precursors in the hydrothermal growth process, and post-growth surface treatment with a Sn precursor solution. In these

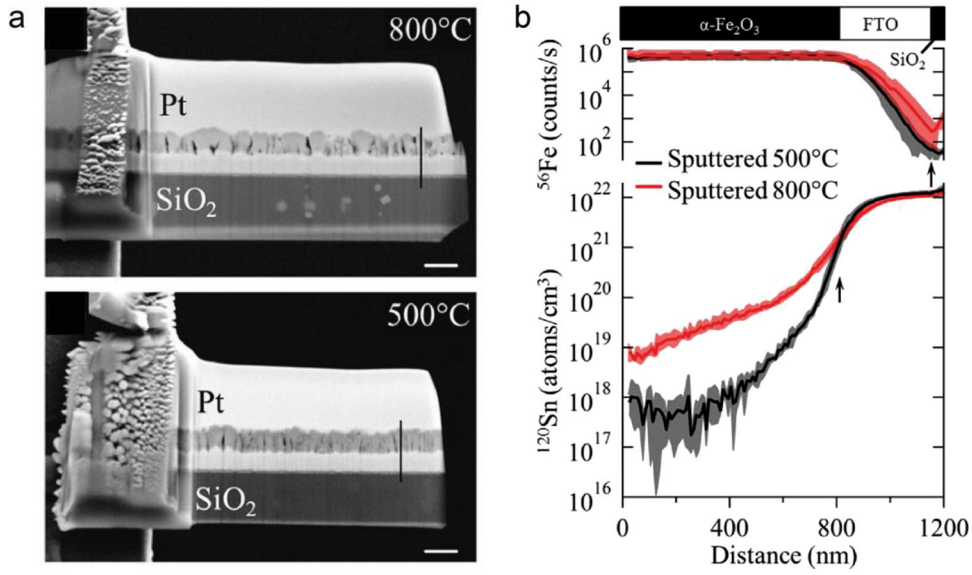

Figure 6. a) SEM images of cross-sectioned hematite sputtered films annealed at 500 °C for 2 h and further annealed at 800 °C for 10 min. Four distinct layers are present: 2000 nm Pt, 600 nm of sputtered hematite, 600 nm of FTO, and float glass. The scale bar in both images is 1 μm. b) Dynamic SIMS of ^{120}Sn and 56Fe from sputtered films of hematite on FTO-coated soda lime float glass annealed at 500 °C for 2 h (black), followed by 800 °C for 10 min (red) assuming a linear sputtering rate. The interface between hematite and FTO is marked by an arrow; the interface between FTO and float glass also is indicated. Quantification is approximate. Shading indicates a single standard deviation calculated from at least three experiments. Reproduced with permission.[92] Copyright 2012, American Chemical Society.

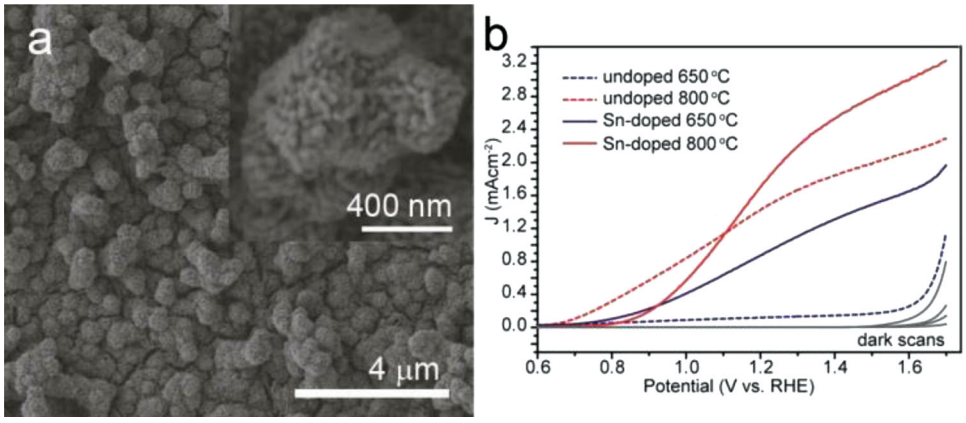

Figure 7. a) SEM images of hematite nanocorals sintered at 650 °C. Inset: High-magnification image shows coral-like nanostructures constituted by small nanorods. b) Comparison of *J–V* scans collected for hematite nanocorals (solid lines) and nanowires (dashed lines) sintered at 650 and 800 °C, with a scan rate of 10 mV s^{-1}, in 1 M NaOH electrolyte (pH 13.6) with the AM 1.5G simulated solar light at 100 mW cm^{-2}. Reproduced with permission.[87] Copyright 2011, American Chemical Society.

previous reports, the role of Sn doping on the electronic and optical properties of hematite nanostructure has been extensively studied. Based on the first-principles calculations within the GGA+*U* approximation, Sn doping can narrow the bandgap of hematite.[91] The incorporated Sn dopants also lead to a lattice distortion of hematite, which enhancing its optical absorption coefficient.[4] Moreover, the enhanced donor density of Sn-doped hematite can reduce the specific resistance.[90]

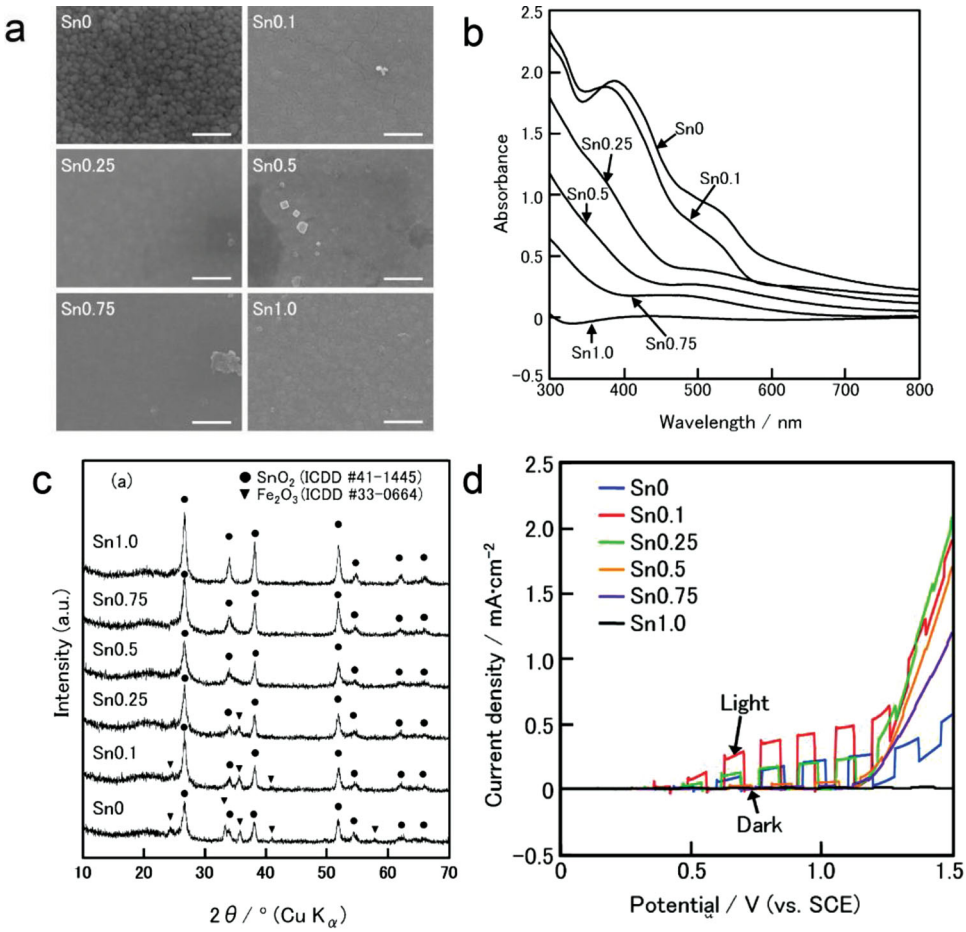

Figure 8. a) SEM images, b) optical absorption spectra, c) XRD patterns measured in wide range of 10–70°, and d) current–potential curves measured under chopped white light for the Fe_2O_3–SnO_2 films prepared on a Nesa silica glass from the solutions of various Sn/(Fe+Sn) mole ratio (denoted as Sn0-Sn1.0 for the Sn ratio from 0 to 1.0). Reproduced with permission.[89] Copyright 2011, American Chemical Society.

These previous works have substantially improved the PEC performance of hematite through Sn doping. However, the interplay between Sn-doping and the performance of hematite photoandes is still not entirely clear. For example, the spatial distribution of Sn dopants in hematite nanostructures is still unclear. It is likely that the Sn-doped hematite samples prepared by the unintentional doping methods will have a gradient of Sn dopant along the growth direction. A hematite photoelectrode with uniform distribution of Sn doping may further optimize its performance. This information could be obtained by using X-ray mapping techniques combined with the SIMS technique to collect the depth profiles of Sn-doped hematite films. Additionally, the effect of increased Sn-dopant on the surface state at the semiconductor/electrolyte interface also needs to be studied, as it will affect the charge transfer kinetics at the interface. Electrochemical impedance spectroscopy (EIS) can be used to investigate the kinetic information of surface-state capacitance, which could lead to a better understanding of the charge collection efficiency and surface oxygen evolution process.[63] Moreover, in situ transient absorption laser spectroscopy can also be carried out to investigate the lifetimes of photoholes and photoelectrons at the timescale of microseconds to seconds, particularly useful to probe the fundamental charge carrier dynamics following photoexcitation. These proposed studies can advance our understanding of the possible effect of Sn doping on the photoexcited electron dynamics in hematite.[93]

The preparation methods and the performance of Sn-doped hematite photoelectrodes can also be further improved. For example, the incorporation of Sn dopant requires high-temperature annealing at 650 °C or above,[90] which is an energy-intensive process that would certainly increase the cost of device fabrication and may damage the growth substrate. Therefore, there is a need to explore new doping methods that can improve the optical and electronic properties of hematite photoanodes for water splitting. Recently, Li and co-workers demonstrated a novel and general strategy to increase the electrical conductivity of hematite by controlled creation of intrinsic dopant such as oxygen vacancy in hematite structure.[55,93] Hydrothermally grown akaganeite (β-FeOOH) nanowire arrays annealed in an oxygen-deficient environment at 550 °C resulted in significantly improved photoactivity for water oxidation, due to the increased donor density resulting from the formation of oxygen vacancies during the thermal decomposition process of akaganeite.[55] This oxygen-deficient thermal decomposition method has further been extended to a two-step low temperature (350 °C) activation process.[94] More importantly, by coupling the inducing oxygen vacancy and element-doping (such as Sn,[94,95] and Ti[72]), the photoactivity of hematite nanostructure was further increased. In spite of the recent progress toward enhancing the photocurrent density, an outstanding challenge for hematite photoanode is the large onset voltage, due to the slow water oxidation kinetics and low lying conduction band.[5,63] It requires a large applied bias typically in the range of 0.8 to 1.0 V vs RHE to obtain photocurrent onset due to the slow water oxidation kinetics.[5,63] It is critical to reduce the over potential of hematite photoanode. Recent advances in the development of heterojunction photoelectrode and oxygen evolution reaction catalysts could potentially address this issue, and further increase the STH efficiency of hematite photoanodes.[63,96–99]

Acknowledgements

Y.L. acknowledges the financial support from University of California, Santa Cruz. Y.C.L. thanks the financial support of Chancellor's Dissertation Year Fellowship at University of California, Santa Cruz.

Received: March 13, 2014
Revised: May 4, 2014
Published online: July 28, 2014

[1] Y. Li, J. Z. Zhang, *Laser Photonics Rev.* **2010**, *4*, 517.
[2] D. A. Wheeler, G. Wang, Y. Ling, Y. Li, J. Z. Zhang, *Energy Environ. Sci.* **2012**, *5*, 6682.
[3] M. Grätzel, *Nature* **2001**, *414*, 338.
[4] K. Sivula, R. Zboril, F. Le Formal, R. Robert, A. Weidenkaff, J. Tucek, J. Frydrych, M. Grätzel, *J. Am. Chem. Soc.* **2010**, *132*, 7436.
[5] K. Sivula, F. Le Formal, M. Grätzel, *ChemSusChem* **2011**, *4*, 432.
[6] G. Wang, Y. Ling, Y. Li, *Nanoscale* **2012**, *4*, 6682.
[7] A. Fujishima, K. Honda, *Nature* **1972**, *238*, 37.
[8] T. Bak, J. Nowotny, M. Rekas, C. C. Sorrell, *Int. J. Hydrogen Energy* **2002**, *27*, 991.
[9] G. Wang, Y. Ling, H. Wang, L. Xihong, Y. Li, *J. Photochem. Photobiol. C* **2014**, *19*, 35.
[10] R. H. Coridan, M. Shaner, C. Wiggenhorn, B. S. Brunschwig, N. S. Lewis, *J. Phys. Chem. C* **2013**, *117*, 6949.
[11] C. Liu, J. Tang, H. M. Chen, B. Liu, P. Yang, *Nano Lett.* **2013**, *13*, 2989.
[12] E. L. Warren, S. W. Boettcher, J. R. McKone, N. S. Lewis, *Proc. SPIE.* **2010**, *7770*,77701F.
[13] H. S. Park, H. C. Lee, K. C. Leonard, G. Liu, A. J. Bard, *ChemPhysChem* **2013**, *14*, 2277.
[14] A. Heller, *Science* **1984**, *223*, 1141.
[15] E. Aharon-Shalom, A. Heller, *J. Electrochem. Soc.* **1982**, *129*, 2865.
[16] S. W. Boettcher, E. L. Warren, M. C. Putnam, E. A. Santori, D. Turner-Evans, M. D. Kelzenberg, M. G. Walter, J. R. McKone, B. S. Brunschwig, H. A. Atwater, N. S. Lewis, *J. Am. Chem. Soc.* **2011**, *133*, 1216.
[17] J. Hensel, G. Wang, Y. Li, J. Z. Zhang, *Nano Lett.* **2010**, *10*, 478.
[18] G. Wang, H. Wang, Y. Ling, Y. Tang, X. Yang, R. C. Fitzmorris, C. Wang, J. Z. Zhang, Y. Li, *Nano Lett.* **2011**, *11*, 3026.
[19] H. Wang, G. Wang, Y. Ling, M. Lepert, C. Wang, J. Z. Zhang, Y. Li, *Nanoscale* **2012**, *4*, 1463.
[20] Y. J. Hwang, C. Hahn, B. Liu, P. Yang, *ACS Nano* **2012**, *6*, 5060.
[21] S. Hoang, S. Guo, N. T. Hahn, A. J. Bard, C. B. Mullins, *Nano Lett.* **2012**, *12*, 26.
[22] S. Hoang, S. P. Berglund, N. T. Hahn, A. J. Bard, C. B. Mullins, *J. Am. Chem. Soc.* **2012**, *134*, 3659.
[23] M. Xu, P. Da, H. Wu, D. Zhao, G. Zheng, *Nano Lett.* **2012**, *12*, 1503.
[24] P. A. DeSario, J. J. Pietron, D. E. DeVantier, T. H. Brintlinger, R. M. Stroud, D. R. Rolison, *Nanoscale* **2013**, *5*, 8073.
[25] M. Ni, M. K. H. Leung, D. Y. C. Leung, K. Sumathy, *Renew. Sust. Energy Rev.* **2007**, *11*, 401.
[26] C. Zhen, L. Wang, L. Liu, G. Liu, G. Q. Lu, H.-M. Cheng, *Chem. Commun.* **2013**, *49*, 6191.
[27] Y. C. Pu, G. Wang, K. D. Chang, Y. Ling, Y. K. Lin, B. C. Fitzmorris, C. M. Liu, X. Lu, Y. Tong, J. Z. Zhang, Y. J. Hsu, Y. Li, *Nano Lett.* **2013**, *13*, 3817.
[28] J. K. Cooper, Y. Ling, C. Longo, Y. Li, J. Z. Zhang, *J. Phys. Chem. C* **2012**, *116*, 17360.

[29] X. Y. Yang, A. Wolcott, G. M. Wang, A. Sobo, R. C. Fitzmorris, F. Qian, J. Z. Zhang, Y. Li, *Nano Lett.* **2009**, *9*, 2331.
[30] G. M. Wang, X. Y. Yang, F. Qian, J. Z. Zhang, Y. Li, *Nano Lett.* **2010**, *10*, 1088.
[31] S. Xie, X. Lu, Y. Tong, *International Photonics and Optoelectronics Meetings (POEM)*, Wuhan, 2013, Optical Society of America, Wuhan **2013**, p. ASa3A.28.
[32] J. Shi, M. B. Starr, H. Xiang, Y. Hara, M. A. Anderson, J. H. Seo, Z. Ma, X. Wang, *Nano Lett.* **2011**, *11*, 5587.
[33] S. Xie, X. Lu, T. Zhai, W. Li, M. Yu, C. Liang, Y. Tong, *J. Mater. Chem.* **2012**, *22*, 14272.
[34] Y. G. Lin, Y.-K. Hsu, Y. C. Chen, L. C. Chen, S. Y. Chen, K. H. Chen, *Nanoscale* **2012**, *4*, 6515.
[35] J. Z. Su, L. J. Guo, N. Z. Bao, C. A. Grimes, *Nano Lett.* **2011**, *11*, 1928.
[36] G. Wang, Y. Ling, H. Wang, X. Yang, C. Wang, J. Z. Zhang, Y. Li, *Energy Environ. Sci.* **2012**, *5*, 6180.
[37] X. Zhang, X. Lu, Y. Shen, J. Han, L. Yuan, L. Gong, Z. Xu, X. Bai, M. Wei, Y. Tong, Y. Gao, J. Chen, J. Zhou, Z. L. Wang, *Chem. Commun.* **2011**, *47*, 5804.
[38] T. Jin, P. Diao, Q. Wu, D. Xu, D. Hu, Y. Xie, M. Zhang, *Appl. Catal. B* **2014**, *148–149*, 304.
[39] V. Cristino, S. Caramori, R. Argazzi, L. Meda, G. L. Marra, C. A. Bignozzi, *Langmuir* **2011**, *27*, 7276.
[40] D. V. Esposito, R. V. Forest, Y. Chang, N. Gaillard, B. E. McCandless, S. Hou, K. H. Lee, R. W. Birkmire, J. G. Chen, *Energy Environ. Sci.* **2012**, *5*, 9091.
[41] C. X. Kronawitter, L. Vayssieres, S. Shen, L. Guo, D. A. Wheeler, J. Z. Zhang, B. R. Antoun, S. S. Mao, *Energy Environ. Sci.* **2011**, *4*, 3889.
[42] K. Sayama, A. Nomura, T. Arai, T. Sugita, R. Abe, M. Yanagida, T. Oi, Y. Iwasaki, Y. Abe, H. Sugihara, *J. Phys. Chem. B* **2006**, *110*, 11352.
[43] G. Wang, Y. Ling, X. Lu, F. Qian, Y. Tong, J. Z. Zhang, V. Lordi, C. Rocha Leao, Y. Li, *J. Phys. Chem. C* **2013**, *117*, 10957.
[44] K. Sivula, *J. Phys. Chem. Lett.* **2013**, *4*, 1624.
[45] M. Zhou, H. B. Wu, J. Bao, L. Liang, X. W. Lou, Y. Xie, *Angew. Chem Int. Ed.* **2013**, *52*, 8579.
[46] F. F. Abdi, L. Han, A. H. M. Smets, M. Zeman, B. Dam, R. van de Krol, *Nat. Commun.* **2013**, *4*, 2195.
[47] J. Su, L. Guo, N. Bao, C. A. Grimes, *Nano Lett.* **2011**, *11*, 1928.
[48] A. Iwase, A. Kudo, *J. Mater. Chem.* **2010**, *20*, 7536.
[49] D. K. Zhong, S. Choi, D. R. Gamelin, *J. Am. Chem. Soc.* **2011**, *133*, 18370.
[50] J. Su, L. Guo, S. Yoriya, C. A. Grimes, *Cryst. Growth Des.* **2009**, *10*, 856.
[51] H. Ye, J. Lee, J. S. Jang, A. J. Bard, *J. Phys. Chem. C* **2010**, *114*, 13322.
[52] Y. Liang, T. Tsubota, L. P. A. Mooij, R. van de Krol, *J. Phys. Chem. C* **2011**, *115*, 17594.
[53] F. F. Abdi, R. van de Krol, *J. Phys. Chem. C* **2012**, *116*, 9398.
[54] G. Wang, Y. Ling, D. A. Wheeler, K. E. N. George, K. Horsley, C. Heske, J. Z. Zhang, Y. Li, *Nano Lett.* **2011**, *11*, 3503.
[55] Y. Ling, G. Wang, J. Reddy, C. Wang, J. Z. Zhang, Y. Li, *Angew. Chem Int. Ed.* **2012**, *124*, 4150.
[56] Y. Lin, S. Zhou, S. W. Sheehan, D. Wang, *J. Am. Chem. Soc.* **2011**, *133*, 2398.
[57] Y. Lin, G. Yuan, S. Sheehan, S. Zhou, D. Wang, *Energy Environ. Sci.* **2011**, *4*, 4862.
[58] L. Li, Y. Yu, F. Meng, Y. Tan, R. J. Hamers, S. Jin, *Nano Lett.* **2012**, *12*, 724.
[59] U. Bjorksten, J. Moser, M. Grätzel, *Chem. Mater.* **1994**, *6*, 858.
[60] S. C. Warren, K. Voatchovsky, H. Dotan, C. M. Leroy, M. Cornuz, F. Stellacci, C. Habert, A. Rothschild, M. Grätzel, *Nat. Mater.* **2013**, *12*, 842.
[61] J. H. Kennedy, M. Anderman, R. Shinar, *J. Electrochem. Soc.* **1981**, *128*, 2371.
[62] N. J. Cherepy, D. B. Liston, J. A. Lovejoy, H. M. Deng, J. Z. Zhang, *J. Phys. Chem. B* **1998**, *102*, 770.
[63] B. Klahr, S. Gimenez, F. Fabregat-Santiago, T. Hamann, J. Bisquert, *J. Am. Chem. Soc.* **2012**, *134*, 4294.
[64] R. H. Goncalves, B. H. R. Lima, E. R. Leite, *J. Am. Chem. Soc.* **2011**, *133*, 6012.
[65] H. L. Wang, J. A. Turner, *J. Electrochem. Soc.* **2010**, *157*, F173.
[66] L. Vayssieres, J. H. Guo, J. Nordgren, *J. Nanosci. Nanotechnol.* **2001**, *1*, 385.
[67] L. Vayssieres, C. Sathe, S. M. Butorin, D. K. Shuh, J. Nordgren, J. H. Guo, *Adv. Mater.* **2005**, *17*, 2320.
[68] J. A. Glasscock, P. R. F. Barnes, I. C. Plumb, N. Savvides, *J. Phys. Chem. C* **2007**, *111*, 16477.
[69] N. T. Hahn, C. B. Mullins, *Chem. Mater.* **2010**, *22*, 6474.
[70] S. Kumari, A. P. Singh, D. Deva, R. Shrivastav, S. Dass, V. R. Satsangi, *Int. J. Hydrogen Energy* **2010**, *35*, 3985.
[71] C. J. Sartoretti, B. D. Alexander, R. Solarska, W. A. Rutkowska, J. Augustynski, R. Cerny, *J. Phys. Chem. B* **2005**, *109*, 13685.
[72] A. Pu, J. Deng, M. Li, J. Gao, H. Zhang, Y. Hao, J. Zhong, X. Sun, *J. Mater. Chem. A* **2014**, *2*, 2491.
[73] J. Liu, C. Liang, H. Zhang, Z. Tian, S. Zhang, *J. Phys. Chem. C* **2012**, *116*, 4986.
[74] R. Franking, L. Li, M. A. Lukowski, F. Meng, Y. Tan, R. J. Hamers, S. Jin, *Energy Environ. Sci.* **2013**, *6*, 500.
[75] S. Shen, C. X. Kronawitter, D. A. Wheeler, P. Guo, S. A. Lindley, J. Jiang, J. Z. Zhang, L. Guo, S. S. Mao, *J. Mater. Chem. A* **2013**, *1*, 14498.
[76] I. Cesar, K. Sivula, A. Kay, R. Zboril, M. Grätzel, *J. Phys. Chem. C* **2009**, *113*, 772.
[77] Y. Q. Liang, C. S. Enache, R. van de Krol, *Int. J. Photoenergy* **2008**, 739864.
[78] V. R. Satsangi, S. Kumari, A. P. Singh, R. Shrivastav, S. Dass, *Int. J. Hydrogen Energy* **2008**, *33*, 312.
[79] M. Zhang, W. Luo, Z. Li, T. Yu, Z. Zou, *Appl. Phys. Lett* **2010**, *97*, 042105.
[80] J. S. Jang, J. Lee, H. Ye, F. R. F. Fan, A. J. Bard, *J. Phys. Chem. C* **2009**, *113*, 6719.
[81] M. Gaudon, N. Pailhe, J. Majimel, A. Wattiaux, J. Abel, A. Demourgues, *J. Solid State Chem.* **2010**, *183*, 2101.
[82] W. B. Ingler, S. U. M. Khan, *Thin Solid Films* **2004**, *461*, 301.
[83] A. Kleiman-Shwarsctein, Y. S. Hu, A. J. Forman, G. D. Stucky, E. W. McFarland, *J. Phys. Chem. C* **2008**, *112*, 15900.
[84] V. M. Aroutiounian, V. M. Arakelyan, G. E. Shahnazaryan, H. R. Hovhannisyan, H. Wang, J. A. Turner, *Sol. Energy* **2007**, *81*, 1369.
[85] L. Xi, S. Y. Chiam, W. F. Mak, P. D. Tran, J. Barber, S. C. J. Loo, L. H. Wong, *Chem. Sci.* **2013**, *4*, 164.
[86] J. S. Jang, K. Y. Yoon, X. Xiao, F. R. F. Fan, A. J. Bard, *Chem. Mater.* **2009**, *21*, 4803.
[87] Y. Ling, G. Wang, D. A. Wheeler, J. Z. Zhang, Y. Li, *Nano Lett.* **2011**, *11*, 2119.
[88] R. Morrish, M. Rahman, J. M. D. MacElroy, C. A. Wolden, *ChemSusChem* **2011**, *4*, 474.
[89] H. Uchiyama, M. Yukizawa, H. Kozuka, *J. Phys. Chem. C* **2011**, *115*, 7050.
[90] J. Frydrych, L. Machala, J. Tucek, K. Siskova, J. Filip, J. Pechousek, K. Safarova, M. Vondracek, J. H. Seo, O. Schneeweiss, M. Grätzel, K. Sivula, R. Zboril, *J. Mater. Chem.* **2012**, *22*, 23232.
[91] X. Meng, G. Qin, W. A. Goddard, S. Li, H. Pan, X. Wen, Y. Qin, L. Zuo, *J. Phys. Chem. C* **2013**, *117*, 3779.
[92] C. D. Bohn, A. K. Agrawal, E. C. Walter, M. D. Vaudin, A. A. Herzing, P. M. Haney, A. A. Talin, V. A. Szalai, *J. Phys. Chem. C* **2012**, *116*, 15290.
[93] M. Barroso, S. R. Pendlebury, A. J. Cowan, J. R. Durrant, *Chem. Sci.* **2013**, *4*, 2724.
[94] Y. Ling, G. Wang, H. Wang, Y. Yang, Y. Li, *ChemSusChem* **2014**, *7*, 848.
[95] T. Y. Yang, H. Y. Kang, U. Sim, Y. J. Lee, J. H. Lee, B. Koo, K. T. Nam, Y. C. Joo, *Phys. Chem. Chem. Phys.* **2013**, *15*, 2117.
[96] F. Le Formal, N. Tetreault, M. Cornuz, T. Moehl, M. Grätzel, K. Sivula, *Chem. Sci.* **2011**, *2*, 737.
[97] C. X. Kronawitter, I. Zegkinoglou, C. Rogero, J. H. Guo, S. S. Mao, F. J. Himpsel, L. Vayssieres, *J. Phys. Chem. C* **2012**, *116*, 22780.
[98] D. K. Zhong, D. R. Gamelin, *J. Am. Chem. Soc.* **2010**, *132*, 4202.
[99] D. K. Zhong, M. Cornuz, K. Sivula, M. Grätzel, D. R. Gamelin, *Energy Environ. Sci.* **2011**, *4*, 1759.